Applied Catalysis B: Environmental 300 (2022) 120739

Contents lists available at ScienceDirect

Applied Catalysis B: Environmental

journal homepage: www.elsevier.com/locate/apcatb

Design of efficient ZnO/ZrO_2 modified CuCoAl catalysts for boosting higher alcohol synthesis in syngas conversion

Chao Huang [a,b], Can Zhu [a,b], Mingwei Zhang [a], Jiangang Chen [a], Kegong Fang [a,*]

[a] State Key Laboratory of Coal Conversion, Institute of Coal Chemistry, Chinese Academy of Sciences, Taiyuan 030001, Shanxi, People's Republic of China
[b] University of Chinese Academy of Sciences, Beijing 100049, People's Republic of China

ARTICLE INFO

Keywords:
CCA|ZnO/ZrO_2 catalysts
Higher alcohols synthesis
Synergetic effect
Mortar-mixing
Syngas conversion

ABSTRACT

Selective synthesis of higher alcohols from syngas conversion is highly desirable, but still very challenging. Here, focusing on the commonly used CuCoAl (CCA) catalyst, we attempted to reconcile the capability of the non-dissociation of CO species and the activation of H_2 through adding ZnO modified ZrO_2 composite into the catalyst for the promotion of higher alcohols synthesis. Under the guidance of such concept, a series of CCA|ZnO/ZrO_2 (m: n) modified catalysts (m: n, represent the mass ratio of ZnO to ZrO_2) were prepared by mortar-mixing CuCoAl and ZnO/ZrO_2 components (2/1 wt ratio). It was found that the CCA|ZnO/ZrO_2 (4:1) catalyst showed a highest total alcohols (ROH) selectivity of 42.6 wt% with excellent C_{2+}OH/ROH fraction of 83.7% among the investigated catalysts. The surface [H*]/[C*] ratio of CCA|ZnO/ZrO_2 catalysts, as revealed by (CO + H_2)-TPD-MS results, increased with the rise of ZnO/ZrO_2 ratio. Moreover, the CCA|ZnO/ZrO_2 (4:1) catalyst with moderate [H*]/[C*] ratio could acquire the highest ROH selectivity and best space time yield of total alcohols (STY_{ROH}) due to that the balance of relative amount of CO*, CH_x* and H* species provided the more probability of C_nH_x*-CO* coupling reaction for higher alcohols synthesis, rather than the hydrogenation reaction of CH_x* or C_nH_x* species and water gas shift reaction.

1. Introduction

Higher alcohols synthesis (HAS) from the direct conversion of syngas (H_2 + CO) originated from coal, natural gas and renewable dry biomass is a promising way to obtain alternative fuels and intermediates for chemical feedstocks [1–4]. This non-petroleum producing route can reduce the dependence of fossil resources and meet the increasing environmental protection requirements, and then have drawn much interest by scientist and engineer till now [2,5,6]. The HAS catalysts mainly included modified Fischer-Tropsch (FT) [5,7,8], modified methanol [9,10], Mo/MoS_2-based [11,12] and Rh-based catalysts [13,14]. Among them, the modified FT catalysts (especially CuCo-based ones) have higher activity and C_{2+} alcohol selectivity at mild reaction conditions, showing a promising potential in practical application. The general consensus is that the dual active sites (Cu and Co species) over CuCo-based catalysts play a crucial role for higher alcohol synthesis, in which the non-dissociative adsorbed CO on Cu^0 sites inserts into the CH_x* species obtained by the hydrogenation reaction of CO dissociative adsorption on Co^0 sites to form higher alcohols [15–17]. The uniform distribution and close contact of dual active sites is considered essential in HAS. For this, Al_2O_3 is usually used as support to highly disperse the Cu and Co active species and strengthen the synergistic catalysis for HAS. As expected, the reported results showed that the higher alcohols selectivity is improved upon Al_2O_3 addition into the CuCo-based catalysts [16,18,19], but it still has large space to meet the practical application in HAS.

To further enhance the higher alcohols selectivity during HAS process, one can attempt to strengthen the probability of non-dissociative adsorbed species (CO*) inserting to alkyl group species over the catalyst during CO hydrogenation. It is well known that ZrO_2 can activate CO and chemically adsorb CO [20,21]. Based on this premise, we consider that ZrO_2 may promote the adsorption of CO and provide the more formation probability of the non-dissociative CO species. However, ZrO_2 has the low ability to dissociate H_2 according to the reported studies [20,21]. The opposite effects of ZrO_2 on CO and H_2 activation usually leads to the low activity for syngas conversion. In our previous work [22], it was found that the CuCoAl|t-ZrO_2 displayed the higher CO adsorption than that of H_2, leading to the lower CO conversion. Moreover, the poor capability of H_2 activation also suppresses the generation of alkyl group species, causing the decreased formation of C_nH_xCO* intermediate

* Corresponding author.
E-mail address: kgfang@sxicc.ac.cn (K. Fang).

https://doi.org/10.1016/j.apcatb.2021.120739
Received 15 August 2021; Received in revised form 16 September 2021; Accepted 17 September 2021
Available online 21 September 2021

species, and then adverse higher alcohol synthesis. Contrarily, ZnO is an effective component to activate H_2 by its heterolytic dissociation [21, 23], providing sufficient active hydrogen species for CO hydrogenation [20]. Therefore, the incorporation of ZnO into ZrO_2 may reconcile capability of CO non-dissociation and H_2 activation, favorable for higher alcohol synthesis in CO hydrogenation.

Recently, Sun's group reported that a CoMn|CuZnAlZr multifunctional catalyst through the physically mixing of CoMn and CuZnAlZr oxides showed a higher oxygenates selectivity in CO hydrogenation [24]. The CoMn oxides provide CO* and C_mH_y* on Co/Co_2C dual active sites, meanwhile the CuZnAlZr oxides offer supplementary CH_xO* species for inserting into C_mH_y* species. Their synergistic effect could virtually suppress C_1 products and enhance higher oxygenates selectivity. Similarly, Luan et al. [25] designed a $ZnCrAlO_x$|KNiMoS-MMO-5 multifunctional catalyst. The $ZnCrAlO_x$ functioned for activating CO to CH_xO* and the KNiMoS-MMO-5 stabilized the CH_xO* intermediates to promote the generation of CH_yCH_xO* species, in which their synergistic effect could effectively acquire better higher alcohols selectivity. Such above research indicated that the multifunctional catalysts can not only keep the inherent characteristics of the two components to a large extent, but also effectively leverage their synergistic effect to enhance the selective synthesis of higher alcohols. Combining the intrinsic nature of ZnO-ZrO_2 on the adsorption and activation for syngas and the advantages of physical mixing method, we presumed that the modified catalyst composed of CuCoAl (CCA) and ZnO-ZrO_2 might strengthen the possibility of non-dissociative CO inserting into alkyl group species to obtain the CH_xCO* intermediate species, favorable for HAS from CO hydrogenation. Additionally, there are few reports on the ZnO-ZrO_2 as a component in CuCoAl-based modified catalyst for higher alcohols synthesis till now.

Therefore, in this paper, a series of modified catalyst (CuCoAl|ZnO/ZrO_2) with varying the ratio of ZnO to ZrO_2 were prepared through a home-made two step procedures. First, the CuCoAl (CCA) and ZnO modified ZrO_2 composite (denoted as ZnO/ZrO_2) were prepared by the co-precipitation and impregnation methods, respectively. Second, the CCA and ZnO/ZrO_2 components were mixed in an agate mortar to form the CCA|ZnO/ZrO_2 composites, which served as effective catalysts for HAS reaction. To better recognize and analyze the structure-activity relationship of the catalysts with different ZnO to ZrO_2 ratio, different characterization techniques including XPS, XRD, BET, TPD (CO, H_2, CO_2, CO+H_2), CO-TPSR and in-situ DRIFTS were performed and discussed in detail to identify the role of ZrO_2, ZnO and ZnO/ZrO_2 in enhancing the catalytic performance, which can deepen the understanding of the HAS reaction mechanism from syngas.

2. Experimental details

2.1. Catalyst preparation

CuCoAl and ZrO_2 were synthesized by the co-precipitation method, which was reported in our previous work [22]. In brief, a 2 M mixed nitrate solution ($Cu(NO_3)_2{\cdot}3H_2O$, $Co(NO_3)_2{\cdot}6H_2O$, $Al(NO_3)_3{\cdot}9H_2O$ and deionized water) together with a 2 M Na_2CO_3 aqueous solution were put into a beaker containing 300 mL deionized water. The resultant precipitate was aged for 2 h under the conditions of continuous stirring, 30 °C and pH = 8.0–8.5. After it was centrifuged and thoroughly washed to the pH of 7, the obtained precipitate was dried at 80 °C overnight, and then calcined in a furnace at 400 °C under static air for 6 h. The as-prepared products were named as CCA (Cu/Co/Al molar ratio of 1:2:1). A 0.35 M $Zr(NO_3)_2{\cdot}5\ H_2O$ solution together with a 2 M Na_2CO_3 aqueous solution were added into a beaker containing 100 mL deionized water under the conditions of 70 ± 1 °C and pH = 10.0 ± 0.5. Then, the above suspension was aged for 3 h. Next, the precipitate was obtained through centrifuging and washing several times to the pH of 7, then drying at 120 °C overnight. Finally, the precipitate was calcinated in a furnace at 550 °C under static air for 3 h.

ZnO modified ZrO_2 (denoted as ZnO/ZrO_2) was fabricated via a method of impregnation. Typically, an $Zn(NO_3)_2$ solution was dropped onto ZrO_2 powder under continuous stirring. Next, the above solution was dried at 100 °C for 4 h under continuous stirring to eliminate H_2O, then dried at 120 °C overnight at static state. Finally, the precursor was calcinated in a furnace at 550 °C under static air for 3 h. The synthesized sample was named as ZnO/ZrO_2 (m:n), in which m:n represent the weight ratio of ZnO and ZrO_2. Additionally, the preparation method of ZnO was similar to that of ZnO/ZrO_2.

ZnO|ZrO_2 was obtained through the physically mixed method with 4/1 wt ratio of ZnO and ZrO_2.

For comparison, a ZnO-ZrO_2 was prepared by the co-precipitation with 4/1 wt ratio of ZnO and ZrO_2. A nitrate solution of zirconium and zinc together with an ammonia solution were added into a beaker of 100 mL deionized water. Then, the above precipitate was aged for 3 h under the conditions of 70 ± 1 °C and pH = 10.0 ± 0.5. Next, the precipitate was got via centrifuging and washing several times to the pH of 7, then drying at 120 °C overnight, and then calcinating at 550 °C for 3 h under static air in a furnace.

The modified composites were synthesized via a mortar mixing technique with 2/1 wt ratio of two components. Briefly, the powdery CCA (CuCoAl) and ZnO/ZrO_2 oxide with a 2/1 wt ratio were grinded in an agate mortar for 40 min, and then pressed, crushed and sieved to 40–60 meshes. The modified composites were denoted as CCA|ZnO/ZrO_2 (m:n). Similarly, the CCA|ZnO|ZrO_2 and CCA|ZnO-ZrO_2 catalysts were synthesized.

The preparation of $CuCoAlZnOZrO_2$, CuCoAlZnO and $CuCoAlZrO_2$ oxides were similar to the above preparation procedures of CuCoAl. Their molar composition is similar to that of CCA|ZnO/ZrO_2 (4:1), CCA|ZnO and CCA|ZrO_2, respectively.

The details of catalyst characterizations and evaluation can be seen in the Supporting Information.

3. Results and discussion

3.1. Catalyst characterization

The XRD detections were performed to reveal the crystal phases of ZnO, ZrO_2, ZnO/ZrO_2, CuCoAl (CCA), as-synthesized and reduced CCA|ZnO/ZrO_2 samples (Fig. 1 and S1). As shown in (Fig. S1), the typical peaks at 2θ of 30.3°, 35.2°, 50.4°, 50.6° and 60.1° for the prepared ZrO_2 are unambiguously indexed to t-ZrO_2 (tetragonal crystal phase, JCPDS # 80–2155) [26]. All ZnO/ZrO_2 samples displays the peaks at 2θ of 31.8°, 34.4°, 36.3°, 47.5°, 56.6°, 62.9°, 66.4°, 68.0° and 69.1°, characteristic of hexagonal ZnO (JCPDS # 36–1451) [27]. The intensity of characteristic diffraction peaks assigned to t-ZrO_2 decrease but those rise for ZnO with increasing ZnO/ZrO_2 ratio, which may be ascribed to the relative larger quantities of ZnO to ZrO_2. Similar phenomenon also occurred for the as-synthesized CCA|ZnO/ZrO_2 catalysts (Fig. 1a). Besides, these catalysts further reveal the presence of two different phases, crystalline $CuCo_2O_4$ (JCPDS # 37–0878) and $CoAl_2O_4$ (JCPDS#38–0814) phases (Fig. 1b). After reduction of the as-synthesized CCA|ZnO/ZrO_2 catalysts at 450 °C, the respective hexagonal ZnO and t-ZrO_2 diffraction peaks were preserved (Fig. 1c), demonstrating that the crystal phase structure is inert or reduced in small quantities during the reduction treatment. For all the reduced CCA|ZnO/ZrO_2 catalysts (Fig. 1d), the diffraction peaks at 2θ of 43.7° between metallic Cu^0 at 43.3° and pure Co^0 at 44.2° are assigned to CuCo alloy phases [17,19], which have the similar crystal size of about 6.8 nm calculated by Scherrer equation. Moreover, the characteristic diffraction peaks of $CoAl_2O_4$ still existed over the sample, suggesting that it was hardly reduced at 450 °C. Based on the above XRD analysis, it could be seen that all the reduced catalysts displayed the same CuCoAl-related crystal structure.

SEM images for ZnO, ZrO_2, ZnO/ZrO_2 samples were shown in Fig. 2, S2 and S3. ZnO sample displays the hexagonal structure (Fig. S2e), which is in agreement with XRD results. For ZnO modified ZrO_2

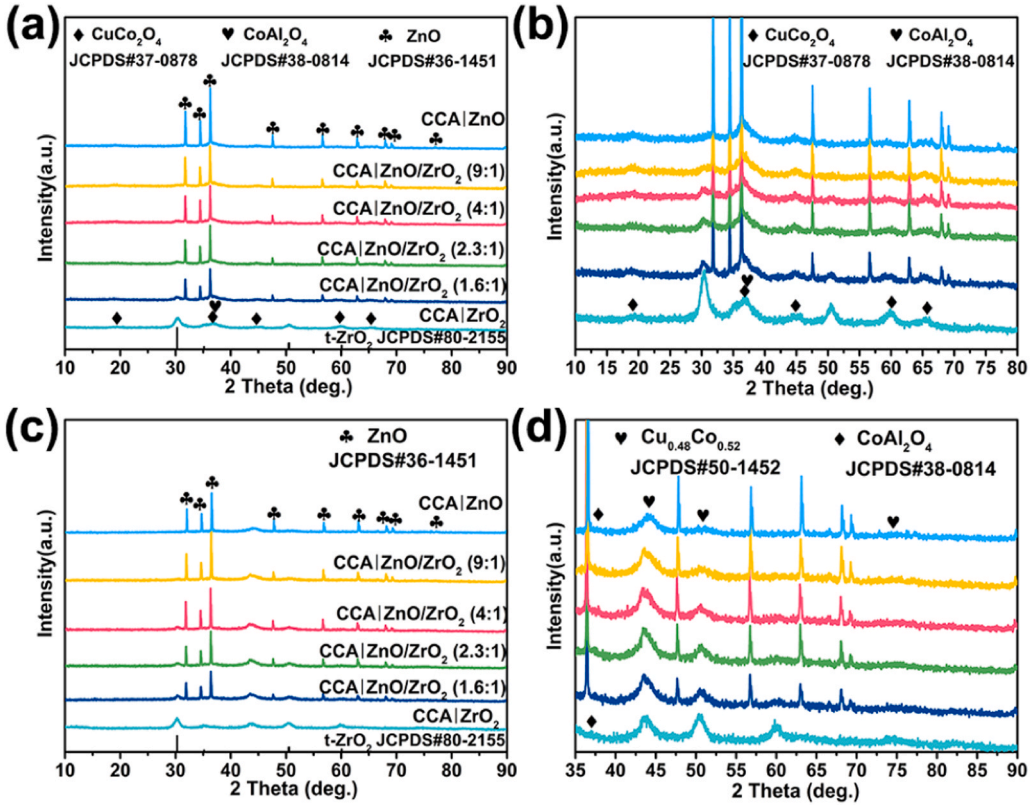

Fig. 1. XRD patterns of CCA|ZnO/ZrO_2 catalysts: (a, b) as-synthesized and (c, d) reduced.

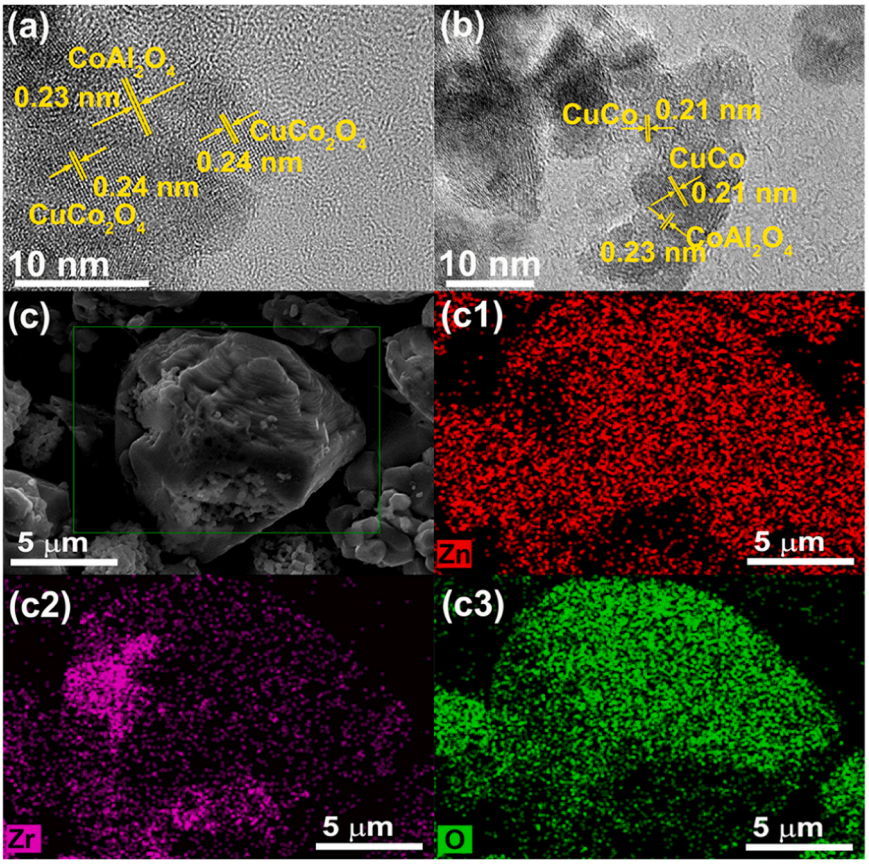

Fig. 2. HRTEM images of as-synthesized (a) and reduced (b) CuCoAl oxides. (c) SEM images of ZnO/ZrO_2 (4:1) with SEM–EDS elemental mapping images for Zn (c1), Zr (c2) and O (c3).

composites with different ZnO/ZrO_2 ratios, the small particles corresponding to ZrO_2 are distributed on ZnO as observed in the SEM image and SEM-EDX elemental mapping images (Fig. 2c and S3). From the TEM images of fresh CuCoAl oxides (Fig. S2a), the dark area including nanofibers and irregularly shaped particles may be the Cu and Co composite oxide, and the light gray area correlates with Al_2O_3. The HRTEM image (Fig. 2a) further depicts that the lattice distances of fresh CuCoAl oxides are about 0.24 and 0.23 nm, corresponding to the lattice planes of the $CuCo_2O_4$ (3 1 1) and $CoAl_2O_4$ (2 2 2) crystal phase, respectively. From the SEM-EDS elemental mapping images (Fig. S2c), the Cu, Co and Al elements are uniformly distributed in CuCoAl oxides. For the reduced CuCoAl oxides (Fig. S2b), a mean particle size of about 10.9 nm is visible. The observed lattice lines in HRTEM (Fig. 2b) are assigned to CuCo alloy (1 1 1) and $CoAl_2O_4$ (2 2 2) crystal phase, respectively, which is accordance to XRD characterization. Furthermore, it is also shown that the CuCo particles are uniformly distributed in Al_2O_3 oxides after reduction. After ZnO/ZrO_2 mixed with CuCoAl oxides (Fig. S4a and b), the morphology and particles size are similar to those of CuCoAl catalyst. As for the fresh CCA|ZnO/ZrO_2 (4:1) catalyst (Fig. S4c), $CuCo_2O_4$ with lattice fringes of 0.24, 0.20 and 0.286 nm was detected. After reduction, the lattice fringe of 0.21 nm assigned to the CuCo alloy was existed (Fig. S4d). Additionally, as shown in the SEM-EDS elemental mapping images (Fig. S5), the intimate contact between ZnO/ZrO_2 and CCA was confirmed.

The N_2 adsorption-desorption isotherms and textural properties of the CCA|ZnO/ZrO_2 catalysts were summarized in Fig. S6 and Table S1. The CCA|ZnO/ZrO_2 catalysts exhibit similar type-IV adsorption isotherms and H2 type hysteresis loop, suggesting its "inkbottle" structure owing to the interparticle space. From Table S1, the CCA sample shows the relatively higher surface area of 116.8 m^2/g. After mixing CCA with ZnO/ZrO_2 samples, the surface area of the samples reduces to 68–82 m^2/g caused by the low surface area of ZnO/ZrO_2.

From the H_2-TPR profiles of ZnO, ZrO_2 and ZnO/ZrO_2 samples (Fig. S7), the slight reduction peaks at ca. 690 °C for ZnO and ca. 735 °C for ZrO_2 are observed. Compared with ZnO and ZrO_2, the ZnO/ZrO_2 samples display a main reduction peak between 440 and 650 °C, which can be contributed to the reduction of ZnO and ZrO_2 [28,29]. Moreover, the area of hydrogen consumption over ZnO/ZrO_2 samples is higher than that of pure ZnO or ZrO_2 and increased with the rise of ZrO_2 content, demonstrating that the combination of ZrO_2 and ZnO makes reduction easier. When the ZnO/ZrO_2 ratio increases, the samples show a decreasing trend of reduction temperature, suggesting the strong interaction between ZnO and ZrO_2. The as-synthesized CCA|ZnO/ZrO_2 catalysts show four main reduction peaks (peak 1, 2, 3 and 4) in the range of 180–700 °C with similar shoulders (Fig. 3), indicating a multi-step reduction process occurred. The lower temperature peak (peak 1) at around 250 °C corresponds to the reduction of Cu^{2+} to Cu^0. The mediate temperature peak (peak 2) at 250–350 °C is ascribed to reduction of Co^{3+} to Co^{2+} and part of Co^{2+} to Co^0 directly. Subsequently, the higher reduction peak (peak 3 and 4) between 350 and 650 °C is mainly responsible for the reduction of Co^{2+} to Co^0 and ZnO/ZrO_2, respectively. The reduction peaks (1 and 2) of CCA|ZnO/ZrO_2 (1.6:1) catalyst is slightly higher than that of CCA|ZrO_2 catalyst, indicating that there might be an interaction between $CuCo_2O_4$ and ZnO, which could hinder the reduction of $CuCo_2O_4$ [30,31]. With the further increase of ZnO content, the reduction peaks (1, 2 and 3) of CCA|ZnO/ZrO_2 catalysts gradually shift to lower temperature, which might be due to the promotion effect of ZnO in H_2 activation, thereby having a significant promotion effect on the reduction process [32]. A possible explanation was that the enhancement effect of ZnO in H_2 activation might be stronger than the inhibitory effect derived from the interaction between $CuCo_2O_4$ and ZnO under the conditions of higher ZnO contents.

The Cu 2p, Co 2p and Al 2p XPS profiles of the reduced CCA|ZnO/ZrO_2 catalysts were shown in Fig. S8. The binding energy (BE) of Cu $2p_{3/2}$ at 931.9–932.5 eV (Fig. S8a) is assigned to Cu^0 as reported in literature [33]. For Co $2p_{3/2}$ (Fig. S8b), the BE at 777.8 − 777.9 eV and 782.5 eV

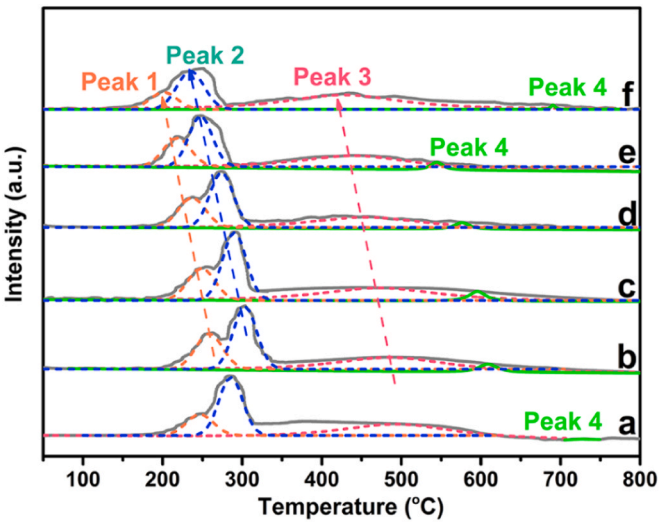

Fig. 3. H_2-TPR profiles of CCA|ZnO/ZrO_2 catalysts: (a) CCA|ZrO_2 catalysts, (b-e) CCA|ZnO/ZrO_2 catalysts with the increase of ZnO/ZrO_2 ratio (1.6:1, 2.3:1, 4:1 and 9:1), (f) CCA|ZnO catalyst.

are ascribed as Co^0 and Co^{2+} species [19,34], demonstrating the feasible existence of $CoAl_2O_4$ phase as reported previously [35]. The BE at 780.4 eV is assigned to CoO species [36,37]. In addition, the BE at about 74 eV of Al 2p (Fig. S8c) confirms the presence of Al_2O_3 in the catalysts [19]. These results are in line with XRD and TEM analysis. The chemical state of Zr and Zn species is shown in Fig. S9. The pattern of Zr $3d_{5/2}$ (Fig. S9a) can be divided into two symmetrical peaks at 181.3 eV and 182.02 eV, attributing to an oxygen-deficient phase of ZrO_2 (Zr_I species) due to the partial reduction of Zr^{4+} towards Zr^{x+} ($x < 4$) and Zr^{4+} state (Zr_{II} species) [38]. The BE Zn 2p at 1021.2–1021.7 eV (Fig. S9b) can be assigned to Zn^{2+} of ZnO [27]. With the increase of ZnO/ZrO_2 ratio, the BE of Zn 2p shifts to lower but Zr 3d to higher values, suggesting the presence of the partial electron transfer among ZnO and ZrO_2 [39]. This further indicated that an interaction between ZnO and ZrO_2 took place as revealed by the H_2-TPR results.

3.2. Catalytic performance

The CCA (CuCoAl), CCA|ZnO, CCA|ZrO_2, CCA|ZnO/ZrO_2 catalysts and ZnO/ZrO_2 were evaluated for HAS reaction under the conditions of 5 MPa, $H_2/CO = 2$, 4000 mL / (g_{cat}.h) and 250 °C (shown in Fig. 4 and Table S2, 3, 4). As shown in Table S3, CCA catalyst displays the higher hydrocarbons (mainly alkane) selectivity of 68.0 wt% but the lower alcohols and CO_2 selectivity of 25.3 and 6.7 wt%, at the CO conversion of 24.7%. As for the HAS performance of ZnO/ZrO_2 catalysts, it can be seen that no HAS performance and a very low CO conversion are observed in Table S4. The ZrO_2 exhibits the higher CO_2 selectivity and lower RH selectivity, which may due to that the ZrO_2 has a stronger ability to activate CO than H_2. Limited H_2 dissociation ability inhibited hydrocarbon generation, and the activated CO was mainly released in the form of CO_2. By contrast, the ZnO displays the highest RH selectivity and lowest CO_2 selectivity, suggesting that ZnO can promote the H_2 activation rather than CO activation. With the rise of ZnO/ZrO_2 ratio, the RH selectivity shows the upward and the CO_2 selectivity exhibits the opposite trend, demonstrating that the ability of CO and H_2 activation can be adjusted by the ZnO/ZrO_2 ratio. Compared with CCA and ZnO/ZrO_2 catalysts, the HAS performance of CCA|ZnO/ZrO_2 catalysts varied distinctively. As shown in Fig. 4a, the CCA|ZrO_2 catalyst shows much lower CO conversion with a large proportion of CO_2 by-product. With the increase of ZnO/ZrO_2 ratio over CCA|ZnO/ZrO_2 catalysts, the CO conversion gradually enhances accompanied by the gradually depressed CO_2 selectivity. The CCA|ZnO catalyst displays highest CO conversion

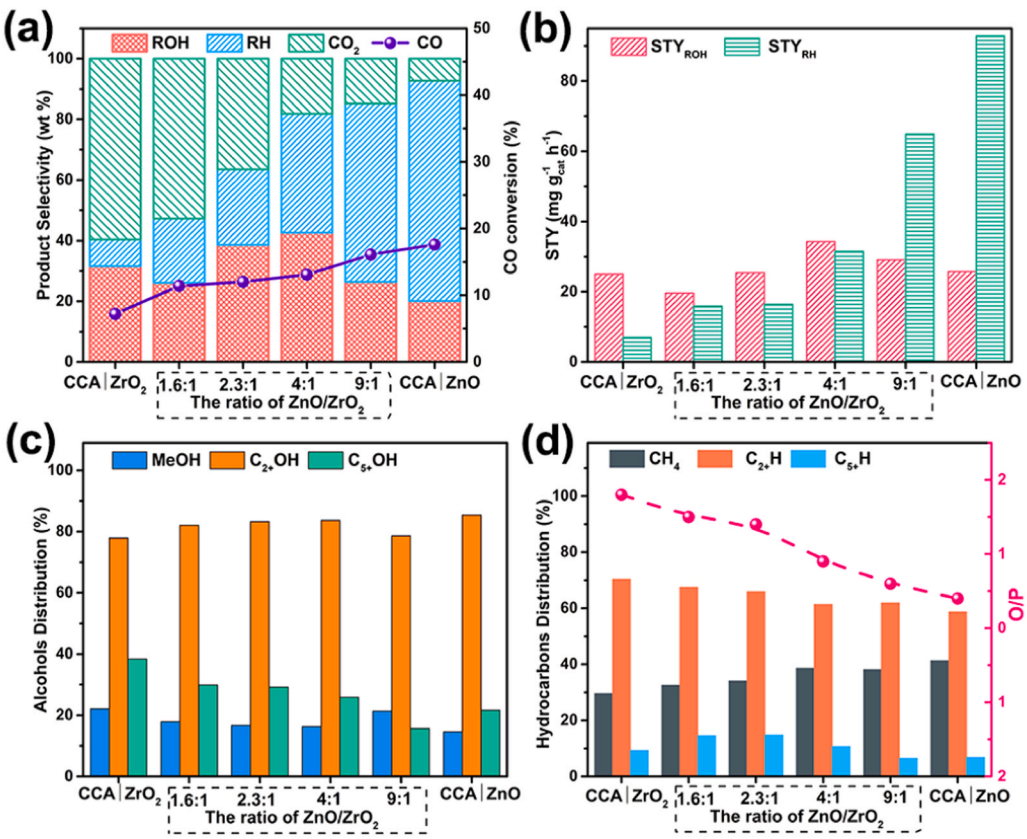

Fig. 4. Catalytic Performance over CCA|ZrO_2, CCA|ZnO/ZrO_2 and CCA|ZnO catalysts for higher alcohols synthesis. (a) ROH, RH and CO_2 selectivity, CO conversion. (b) The space-time-yield (STY) of ROH and RH. (c) Alcohols distribution. (d) Hydrocarbons distribution and O/P (the ratio of olefins/paraffins) Reaction conditions: 5.0 MPa, 250 °C, 4000 mL / (g_{cat}·h), n(H_2)/n(CO) = 2. $C_{2+}H$: the hydrocarbons with two or more than carbon numbers. $C_{5+}H$: the hydrocarbons with five or more than carbon numbers.

(17.6%), lowest ROH and CO_2 selectivity (20.1 and 7.4 wt%). This result suggested that the catalytic activity was promoted under the higher ZnO/ZrO_2 ratio in CCA|ZnO/ZrO_2 catalysts, while the CO_2 selectivity was suppressed. The ROH selectivity and space-time-yield (STY_{ROH}) over CCA|ZnO/ZrO_2 catalysts (shown in Fig. 4a and b) exhibit a volcanic trend with the increase of ZnO/ZrO_2 ratio. When the ZnO/ZrO_2 ratio is 4:1, the catalyst (CCA|ZnO/ZrO_2 4:1) displays the highest ROH selectivity and STY_{ROH}. The above results revealed that a proper ZnO/ZrO_2 ratio over CCA|ZnO/ZrO_2 catalysts was crucial to the higher alcohol synthesis and CO_2 suppression. Excessive or much lower ZnO/ZrO_2 ratio is detrimental to the production of higher alcohols because of the superfluous hydrogenation or WGS reaction.

The product distributions of alcohols and hydrocarbons on the selected catalysts were further investigated in Fig. 4c and d. The $C_{5+}OH$ contents in ROH decreased with the increase of ZnO/ZrO_2 ratio, demonstrating that the introduction of ZnO was harmful to the ability of carbon chain growth and then suppressed the formation of heavier carbon alcohols. As far as hydrocarbon distribution was concerned (seen Table S2), the $C_{2+}H$ and $C_{5+}H$ contents decreased but the CH_4 content enhanced with the rise of ZnO/ZrO_2 ratio, indicating that the introduction of ZnO could weaken the ability of carbon chain growth. Besides, the decrease of the olefin/paraffin ratio in hydrocarbons (denoted as O/P) is accompanied by an increase of CH_4 content, revealing the promotion of hydrogenation reaction upon ZnO addition. The quasi-Anderson-Schulz-Flory (ASF) plots of ROH and RH were presented in Fig. S10 and S11. It could be seen that the alcohols distributions over all CCA|ZnO/ZrO_2 catalysts conformed the classical Anderson-Schulz-Flory (ASF) model (Fig. S10). Notably, the carbon chain growth probability (α) of alcohols calculated through fitting the quasi-ASF plots with ten carbons numbers to acquire the slope decreased with the increase of ZnO/ZrO_2 ratio. The higher carbon chain growth probability of CCA|ZrO_2 catalyst was favorable for the production of $C_{5+}OH$. In contrast, the CCA|ZnO catalyst tended to the production of the lower carbon alcohols. Similarly, the carbon chain growth probability (α) for hydrocarbons also reduced as the ratio of ZnO/ZrO_2 increased (Fig. S11). These results further revealed that ZnO addition could weaken the carbon chain growth probability of alcohols and hydrocarbons.

Since the ZnO/ZrO_2 composites had the significant influence on the catalytic performance of CCA|ZnO/ZrO_2 catalyst as discussed above, we further surveyed the different preparation method of ZnO-ZrO_2 composite with ZnO/ZrO_2 ratio of (4:1), including physically mixing (ZnO|ZrO_2), impregnation (ZnO/ZrO_2) and co-precipitation (ZnO-ZrO_2). The subsequent obtained CCA|ZnO|ZrO_2, CCA|ZnO/ZrO_2 and CCA|ZnO-ZrO_2 catalysts and their catalytic performance were exhibited in Fig. 5. The CCA|ZnO|ZrO_2 catalyst gave a ROH selectivity (34.1 wt%) with $C_{2+}OH$ and $C_{5+}OH$ contents in total alcohols of 75.5% and 18.1% at CO conversion of 10.6%. Meanwhile, the much higher CO_2 selectivity (32.4 wt%) was also observed. The CCA|ZnO/ZrO_2 catalyst afforded the higher ROH selectivity of 42.6 wt% (with 83.7% $C_{2+}OH$ content in alcohols) and CO conversion (13.1%) with the sharp drop of CO_2 selectivity (18.2 wt%). Comparatively, the CCA|ZnO-ZrO_2 catalyst displays the comparable 15.5% CO conversion but sharply decreasing ROH selectivity (22.1 wt%) with a highest $C_{2+}OH$ contents (90.3%) as well as the lowest CO_2 selectivity (4.9 wt%). As to the hydrocarbon distribution (Table S5), the CCA|ZnO/ZrO_2 catalyst also shows the lower CH_4 content than that of CCA|ZnO|ZrO_2 and CCA|ZnO-ZrO_2 catalysts. As for the space-time-yield (STY) of ROH, it was much higher over the CCA|ZnO/ZrO_2 catalyst than that on the CCA|ZnO|ZrO_2 and CCA|ZnO-ZrO_2 catalysts. Obviously, the above results demonstrated that the CCA|ZnO/ZrO_2 catalyst displayed the excellent ROH selectivity and STY_{ROH} among the investigated catalysts. For better comparison, three additional catalysts (CuCoAlZnOZrO_2, CuCoAlZnO and CuCoAlZrO_2) were synthesized by the co-precipitation. Compared with CuCoAlZnO and CuCoAlZrO_2, the CuCoAlZnOZrO_2 catalyst exhibits the better ROH selectivity (Table S6), suggesting that ZnOZrO_2 composite can enhance the ROH selectivity of CuCoAl catalyst. However, its ROH selectivity, $C_{2+}OH$ and $C_{5+}OH$ in

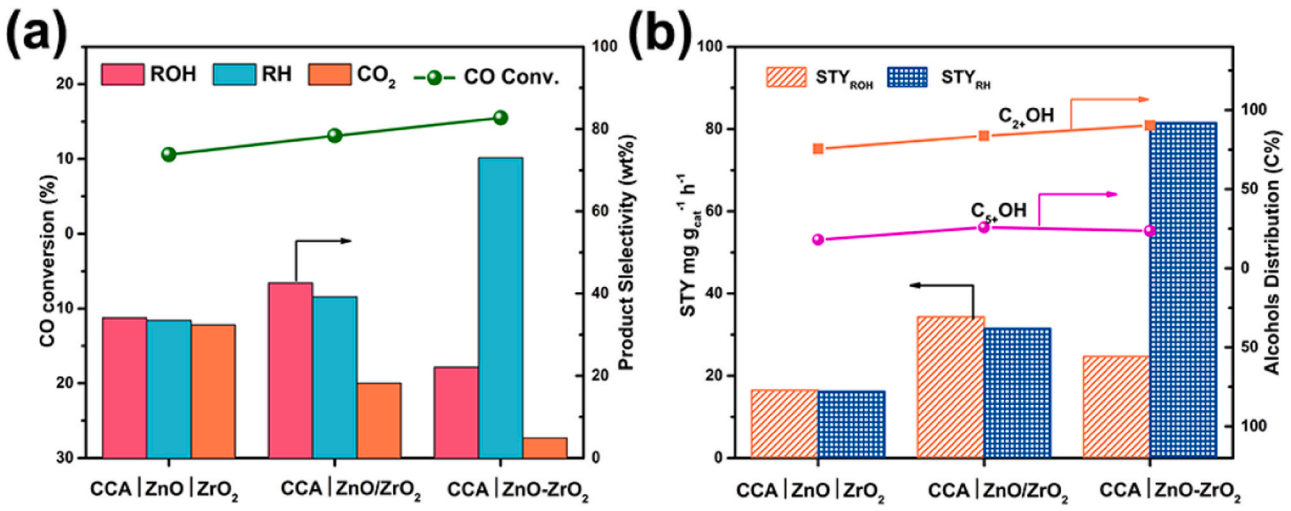

Fig. 5. Catalytic performance of CCA|ZnO/ZrO_2, CCA|ZnO|ZrO_2 and CCA|ZnO-ZrO_2 catalysts. (a) CO conversion, CO_2, ROH and RH selectivity. (b) The space-time-yield (STY) for ROH and RH and alcohols distribution. Reaction conditions: 5 MPa, 250 °C, 4000 mL / (gcat.h), n(H_2)/n(CO) = 2.

alcohols distribution are still lower than that of CCA|ZnO/ZrO_2 (4:1) catalyst. In contrast to CuCoAlZnOZrO_2 catalyst prepared by co-precipitation, the CCA|ZnO/ZrO_2 (4:1) catalyst obtained by the physically mixing of CCA and ZnO/ZrO_2 (4:1) could maintain the inherent properties of the two components to a certain extent, and effectively exerted their synergistic effect to improve HAS performance.

3.3. Reactivity of surface Cu and Co active sites

The CO-TPSR-MS analysis was conducted to investigate the surface reactivity of CCA|ZnO/ZrO_2 catalysts. The *m/z* of 15, 44, 2 and 46 represent CH_4, CO_2, H_2 and HCOOH species [40], respectively. The CH_4 formation over CCA| ZnO/ZrO_2 catalysts exhibit one major peak in 170–450 °C (Fig. S12a), due to the hydrogenation of surface C* caused by H-assisted CO dissociation [41]. In CO-TPSR profiles, the temperature of the maximum CH_4 formation could be represented the intrinsic catalytic activity [42]. Generally, the catalyst with lower temperature of the maximum CH_4 formation could display the higher catalytic activity. With the increase of ZnO/ZrO_2 ratio, the aforesaid temperature basically shows a downward trend, implying the enhancement of the catalyst activity. This was in good accordance to the trend observed in HAS reaction (Fig. 4a). In addition, it also shows that the temperature of the major hydrogen consumption peak decreases as the ZnO/ZrO_2 ratio increases (Fig. S12c), suggesting that the hydrogenation reaction was conducive to occur on the CCA|ZnO/ZrO_2 catalyst with higher ZnO content. The formation of HCOOH species over all the samples could be observed in Fig. S12d. As reported in literatures [18,27,43], the formate species (HCOOH) is a critical C_1 species for HAS. Other research considered that it was also a key intermediate in WGS reaction [44,45]. Notably, HCOOH and CO_2 show the similar peak type and desorption temperature (Fig. S12b and d), indicating that the HCOOH species is an important intermediate in higher alcohols and CO_2 formation over the CCA|ZnO/ZrO_2 catalyst.

3.4. Structure-performance relationship

Although ZrO_2 could chemically adsorb and activate CO, the CCA|ZrO_2 modified catalyst exhibited low CO conversion and high CO_2 selectivity due to its poorer ability of activating H_2 than CO. After ZnO modified ZrO_2, the CCA|ZnO/ZrO_2 modified catalysts exhibited the increasing CO conversion, higher alcohols formation and decreasing CO_2 selectivity. Such differences in catalytic performance would be derived from the discrepancies of the intrinsic physicochemical properties of the samples. For clarifying the structure-performance relationship, we further analyzed the surface basicity, CO and H_2 chemisorption behaviors of the catalysts.

3.4.1. Surface basicity

The CO_2-TPD-MS experiments of CCA|ZrO_2, CCA|ZnO/ZrO_2 and CCA|ZnO catalysts were carried out to investigate their basic properties. There were three types of desorption peaks: low (α, <150 °C), medium (β, 150–350 °C) and high (γ, 350–470 °C) temperature peaks over all the catalysts (Fig. 6a), corresponding to the weak, medium-strength and strongly basic sites. In general, the weak basic sites (peak α) are described as the adsorption of CO_2 on surface OH groups. [46] The medium-strength basic sites (peak β) are assigned to M^{n+}-O^{2-} pairs (M = Zr or Al). [46] The strongly basic sites (peak γ) are usually relevant to the unsaturated O^{2-} anion. [46,47] The temperature of desorption peak (peak α, β and γ) gradually decreased with the increase of ZnO/ZrO_2 ratio (Fig. 6b), implying that the basicity of CCA|ZnO/ZrO_2 catalysts was weakened during this changing course. Combining with the catalytic performance of CCA|ZnO/ZrO_2 catalysts, it could deduce that the moderate basicity of CCA|ZnO/ZrO_2 (4:1) enhanced the higher alcohols selectivity.

3.4.2. Chemisorption behaviors of syngas (H_2 + CO)

The actual adsorption behaviors of CO and H_2 over the CCA|ZnO/ZrO_2 catalysts under the reaction atmosphere were further examined by using the (H_2 + CO)-TPD-MS experiment (see Fig. 7). The desorption profiles of CO can be divided into three desorption zone (Fig. 7a), corresponding to physiosorbed CO desorption (CO_I, around 100 °C), non-dissociative adsorption CO (CO_{II}, 170–430 °C) and dissociative adsorption CO (CO_{III}, 430–800 °C). Compared to CO-TPD experiments (Fig. S13), the peak area of CO_{III} for all the CCA|ZnO/ZrO_2 catalysts is higher than that of CO-TPD results (shown in Table S7). Furthermore, different from the CO-TPD experiments, the relationship between the chemical desorption area of CO (CO_{II} + CO_{III}) and ZnO/ZrO_2 ratio is not linear, demonstrating that the presence of H_2 promoted CO dissociation [42] and thereby increasing the desorption of CO_{II} + CO_{III}.

In term of the desorption profiles of H_2 (Fig. 7b), the curve was described as the lower temperature zone (H_I) and higher temperature zone (H_{II}). The H_I is usually attributed to the H species adsorbed on the metal (Cu, Co and Zn) surface, while the H_{II} is assigned to the spillover H on the support. As ZnO/ZrO_2 ratio increased, the desorption area of H_2 showed the upward trend (Fig. 7c), implying that the ZnO addition enhanced H_2 adsorption, which was consistent with the H_2-TPD experiments (shown in Fig. S14). Moreover, combining with the basicity of CCA|ZnO/ZrO_2 catalysts revealed by the CO_2-TPD characterization, we

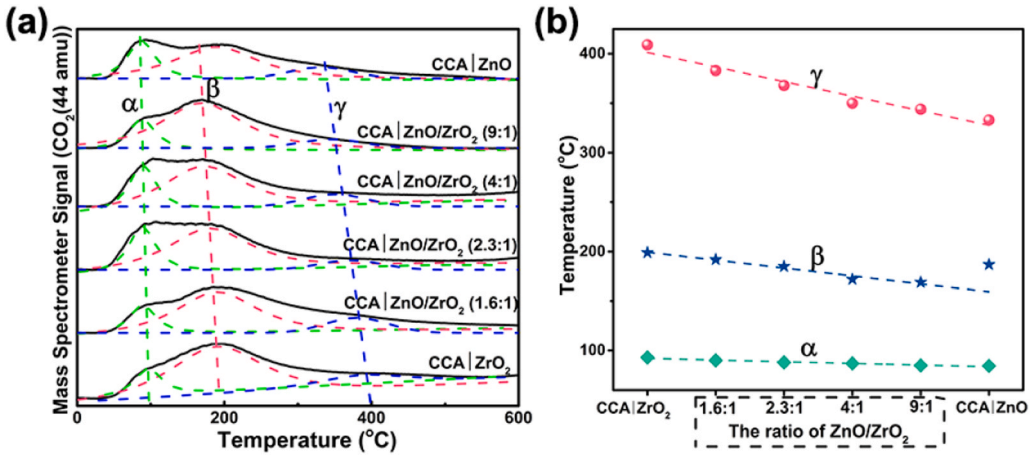

Fig. 6. **(a)** CO_2-TPD-MS profiles of CCA|ZnO/ZrO_2 catalysts. (b) The desorption temperature of CCA|ZnO/ZrO_2 catalysts.

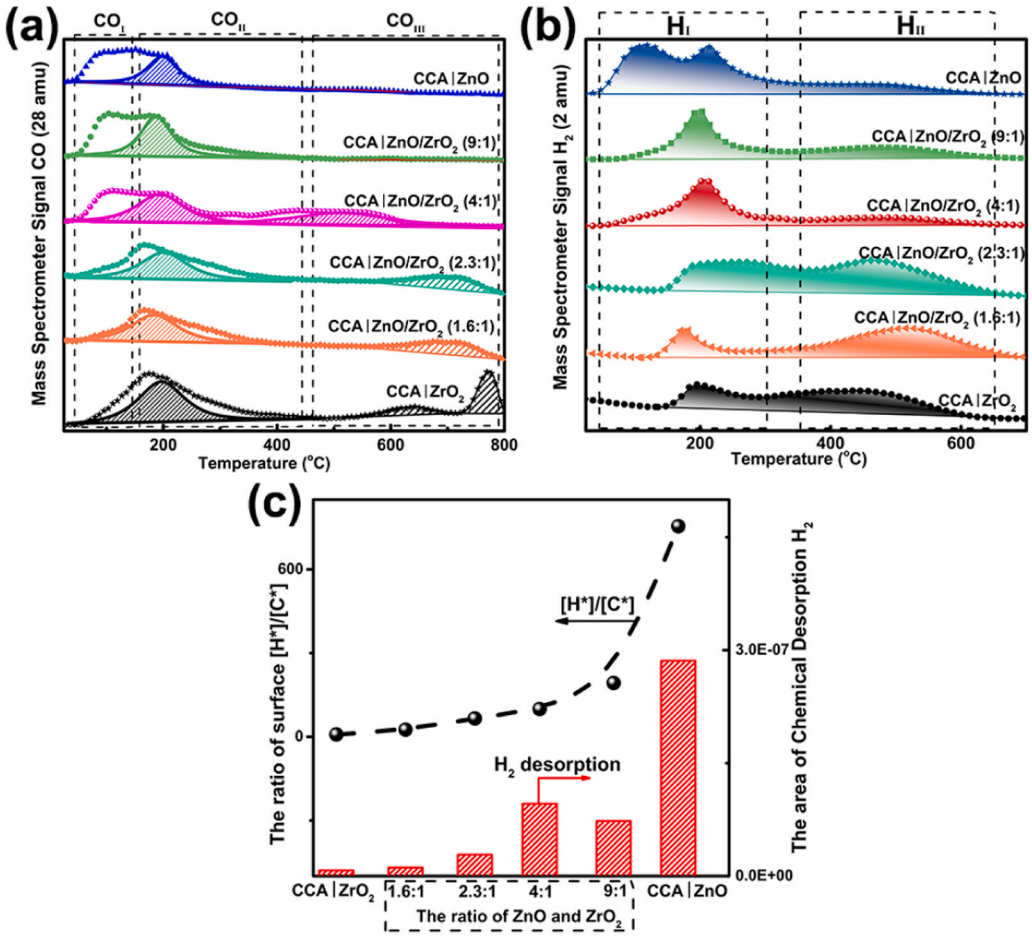

Fig. 7. (H_2 + CO)-TPD-MS experiment of CCA|ZnO/ZrO_2 catalysts: the desorption of (a) CO, (b) H_2, (c) The area of chemical desorption H_2 and the ratio of surface [H*]/[C*].

presumed that the weaker basicity at higher ZnO/ZrO_2 ratio could strengthen H_2 adsorption of the catalysts. Similar promotion of H_2 adsorption phenomenon aroused from the decreasing basicity on alkali metal promoted iron catalysts was also observed [48]. On the basis of above analysis, the adsorption behaviors of CO and H_2 in syngas atmosphere differed with that of pure CO or H_2, demonstrating that a competition adsorption of CO and H_2 occurred on the active sites of CCA|ZnO/ZrO_2 catalysts.

Based on the desorption area of chemisorption H_2 and CO of (H_2 + CO)-TPD-MS, we calculated the ratio of twice desorption area of H_2 to desorption area of CO (denoted as surface [H*]/[C*] ratio). From Fig. 7c, it can be seen that the addition of ZnO greatly increased the surface [H*]/[C*] ratio, following the order of CCA|ZrO_2 < CCA|ZnO/ZrO_2 (1.6:1) < CCA|ZnO/ZrO_2 (2.3:1) < CCA|ZnO/ZrO_2 (4:1) < CCA|ZnO/ZrO_2 (9:1) < CCA|ZnO. Fig. 8 further outlines the close relationship between STY_{ROH}, ROH, CO_2 selectivity, C_{5+}OH/ROH and O/P and

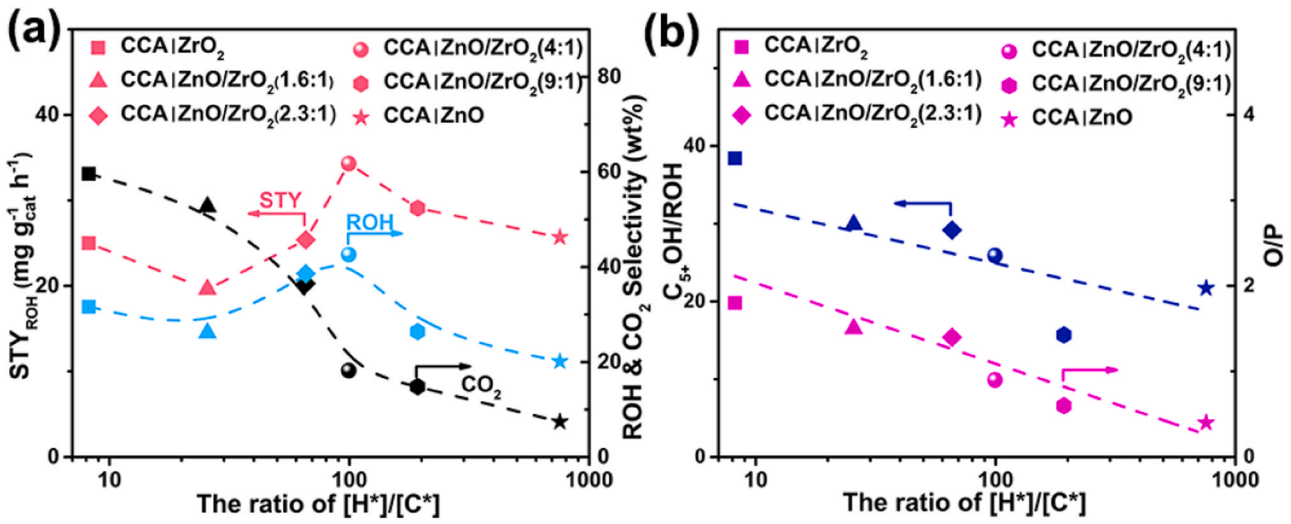

Fig. 8. The relationship of catalytic performance and [H*]/[C*] ratio. (a) STY_{ROH}, ROH and CO_2 selectivity to [H*]/[C*] ratio. (b) $C_{5+}OH$/ROH and O/P to [H*]/[C*] ratio.

surface [H*]/[C*] ratio. With the increase of surface [H*]/[C*] ratio, the STY_{ROH} and ROH selectivity presents a volcanic trend with decreasing trend in CO_2 selectivity, $C_{5+}OH$/ROH and O/P ratio (Fig. 8). But the CH_4 contents in hydrocarbons monotonously increased in this varying process. It had been reported that the [H*]/[C*] ratio played a significant role in determining the product synthesis of CO hydrogenation [49,50]. The higher surface [H*] concentration would enhance the formation of C* species from H-assisted CO dissociation rather than CO* species, thus leading to the more CH_x species. The concentration of active CH_x species available for hydrocarbon synthesis was relatively higher, thereby resulting in the larger amount of hydrocarbon products. Moreover, the higher [H*]/[C*] ratio also provided more opportunities for the hydrogenation reaction, facilitating chain termination reaction and the generation of low-carbon alkanes at the expense of alcohols and CO_2 formation. As expected, CCA|ZnO catalyst exhibited the lower O/P ratio, ROH, CO_2 selectivity and higher CH_4 selectivity due to the highest surface [H*]/[C*] ratio. On the contrary, the CCA|ZrO_2 catalyst possessed the lowest surface [H*]/[C*] ratio and the amount of H_2 adsorption. Thus, the H-assisted CO dissociation was suppressed and then more CO* species was formed, which was the prerequisite for the generation of alcohols and CO_2. However, due to the lack of sufficient CH_x* species, the abundant CO* species were released in the form of CO_2, which came from water shift gas reaction ($CO + H_2O \rightarrow CO_2 + H_2$), causing the unsatisfying ROH selectivity and STY_{ROH} over the CCA|ZrO_2 catalyst. Even though the catalytic evaluation of the CCA|ZrO_2 catalyst and CCA|ZnO catalyst under higher or lower H_2/CO syngas were performed (Table S8), the satisfying ROH selectivity was not acquired. Therefore, in terms of ZrO_2 or ZnO individually modified CCA catalysts, it was difficult to achieve superior alcohol selectivity by adjusting H_2/CO ratio of syngas due to the lacking of their synergetic effect.

As for higher alcohols synthesis, it was widely considered that non-dissociative CO adsorption (CO*) inserted into the CH_x* species to obtain acyl intermediates (CH_xCO*), and finally forming higher alcohols. Thus, the balance of the relative concentration of CO*, CH_x* and H* species was critical for higher alcohols synthesis. Both the highest and lowest surface [H*]/[C*] ratio was not benefit to the formation of higher alcohols upon lacking the necessary amount of CO* species or CH* species. In the present study, the STY_{ROH} and ROH selectivity over CCA|ZnO/ZrO_2 catalysts presented a volcanic trend as the surface [H*]/[C*] ratio increased. At ZnO/ZrO_2 ratio of 4:1, the CCA|ZnO/ZrO_2 (4:1) catalyst displayed the highest ROH selectivity and STY_{ROH} due to the balance of relative amount of CO*, CH_x* and H* species at the moderate surface [H*]/[C*] ratio, which coincided with the above analysis for higher alcohols synthesis. In summary, the suitable surface [H*]/[C*] ratio of CCA|ZnO/ZrO_2 catalyst could be adjusted by the ZnO/ZrO_2 ratio and then achieved the excellent ROH selectivity and STY_{ROH}.

Additionally, the surface [H*]/[C*] ratio also had a significant influence on determining alcohols distribution in HAS reaction. Li. et al. [51] considered that a lower H_2/CO ratio could effectively inhibit the occurrence of chain termination and improve the ability of carbon chain growth, which was conducive to the formation of heavier products. For our investigated catalysts, the increase of surface [H*]/[C*] ratio boosted the occurrence of chain termination, thus unfavorable for the formation of $C_{5+}OH$. Consequently, CCA|ZrO_2 catalyst with lower surface [H*]/[C*] ratio had weak capability of the chain termination, and obtained the more production of $C_{5+}OH$. In contrast, the CCA|ZnO/ZrO_2 catalysts with higher surface [H*]/[C*] ratio produced less formation of $C_{5+}OH$.

4. Reaction mechanism on CCA|ZnO/ZrO_2 catalyst

In situ DRIFTS under syngas ($CO/H_2 = 1/2$) flow was performed to investigate the differences in CO adsorption types for ZnO, ZnO/ZrO_2 (4:1) and ZrO_2. As shown in Fig. 9a, b, c and d, the gaseous CO (2171, 2115 cm^{-1}) [52] and linear-type adsorbed CO (2034 cm^{-1}) [16] are observed. The peaks at 1991 and 1801 cm^{-1} are ascribed to the bridge-type adsorbed CO and multi-bonded adsorbed CO [22,53,54], respectively. For ZnO/ZrO_2 (4:1) and ZrO_2 samples, the intensity of linear-type, bridge-type and multi-bonded adsorbed CO obviously increased (Fig. 9a, b and d) with the increase of temperature from 50 to 250 °C. However, almost no CO adsorption was detected on ZnO sample (Fig. 9c and d), which indicates that it has a poor ability to activate CO. Notably, those characteristic peaks intensity followed the order: ZrO_2 > ZnO/ZrO_2 (4:1) > ZnO, implying the consistent sequence of activating CO capacity for the samples. The syngas desorption behaviors of ZnO, ZnO/ZrO_2 (4:1) and ZrO_2 after reaction by in situ DRIFTS also verified the similar result mentioned above (Fig. 9e). CO and H_2 chemisorption analysis were carried out to gain the information about CO and H_2 activation of ZnO, ZnO/ZrO_2 (4:1) and ZrO_2, as shown in Fig. 10. Compared with ZnO sample, the ZrO_2 and ZnO/ZrO_2 (4:1) displayed the relatively stronger CO adsorption capacity (Fig. 10a), suggesting that the latter possessed better activating CO ability. This result was well in accordance to the above in situ DRIFTS analysis. As shown in Fig. 10b, the H_2 adsorption area of ZnO was higher than that of ZrO_2 and ZnO/ZrO_2 (4:1), implying that H_2 activation could be promoted by ZnO rather than ZrO_2. In summary, an equilibrium was

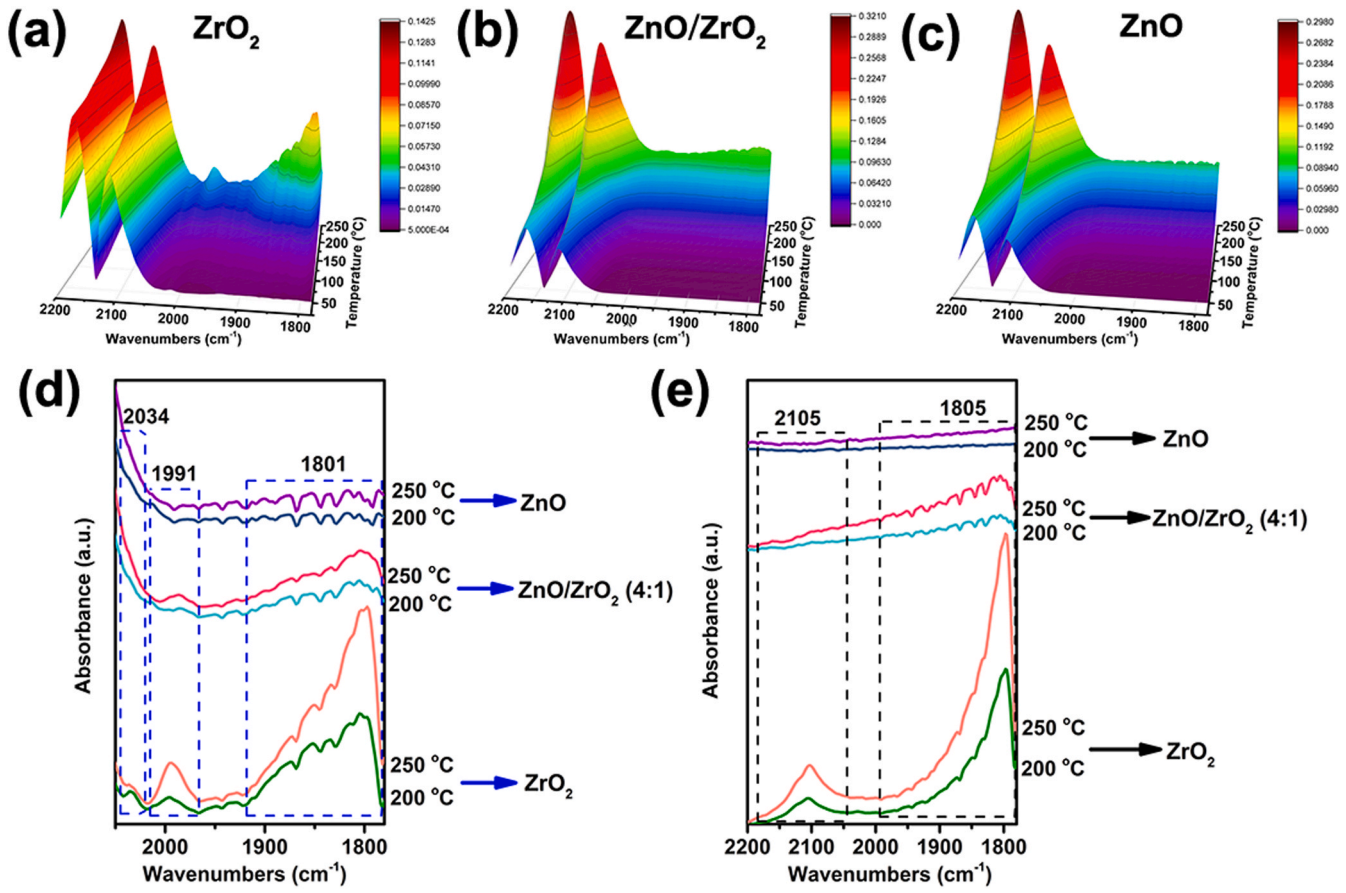

Fig. 9. In situ DRIFTS spectra of syngas ($CO/H_2 = 1/2$) flow on different reduced catalysts: (a) ZrO_2; (b) ZnO/ZrO_2 (4:1); (c) ZnO; (d) The different types of CO adsorption on ZnO, ZnO/ZrO_2 (4:1) and ZrO_2. (e) In situ syngas ($CO/H_2 = 1/2$) DRIFTS spectra of N_2 flow on ZnO, ZnO/ZrO_2 (4:1) and ZrO_2.

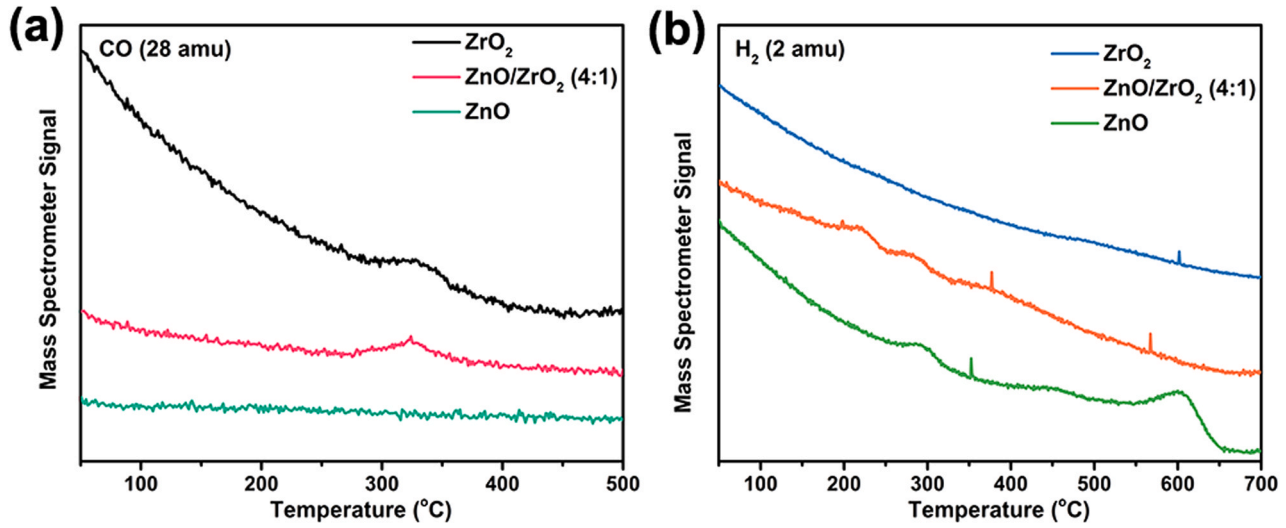

Fig. 10. (a) CO-TPD-MS and (b) H_2-TPD-MS profiles of ZnO, ZnO/ZrO_2 (4:1) and ZrO_2.

obtained on ZnO/ZrO_2 (4:1) sample, with a balanced ability to activate H_2 and CO.

The difference in CO activation types over CCA|ZnO/ZrO_2 catalysts were also investigated by in situ DRIFTS (Fig. 11a). The absorption band between 2250 and 2050 cm^{-1} is ascribed to gaseous CO. Moreover, the linear-type (around 2030 cm^{-1}), bridge-type (2020–1912 cm^{-1}) and multi-bonded adsorbed CO (1912–1700 cm^{-1}) are observed, and they all become stronger as the temperature increases. The relative intensity of multi-bonded and bridge-type adsorbed CO was calculated by the formula of $I_{multi\text{-}bonded/bridge\text{-}type} = I_{multi\text{-}bonded} / I_{bridge\text{-}type}$ (I represents the relative intensity of characteristic peak, see Fig. S15). As shown in Fig. 11b, the $I_{multi\text{-}bonded/bridge\text{-}type}$ followed the order: CCA|ZrO_2 > CCA|ZnO/ZrO_2 (4:1) > CCA|ZnO. The CO adsorption over CCA|ZrO_2 catalyst mainly existed in the form of multi-bonded adsorbed CO, while the

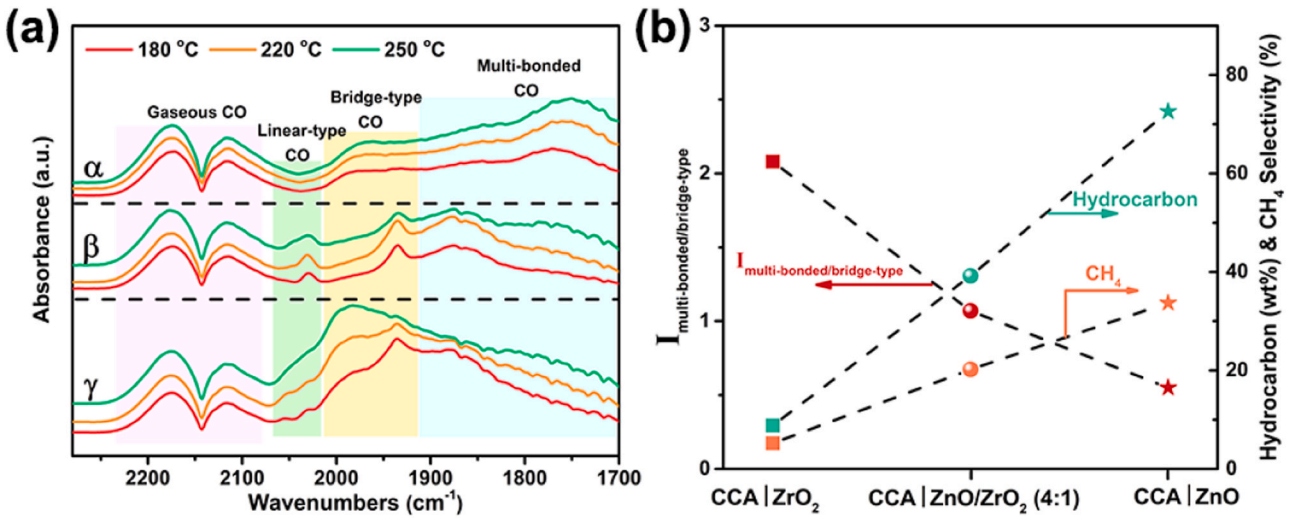

Fig. 11. (a) In situ DRIFTS spectra of syngas (CO/H_2 = 1/2) flow on different reduced catalysts: (α) CCA|ZrO_2; (β) CCA|ZnO/ZrO_2 (4:1); (γ) CCA|ZnO. (b) The relationship between $I_{multi\text{-}bonded/bridge\text{-}type}$ and hydrocarbon or CH_4 selectivity under the reaction temperature of 250 °C. $I_{multi\text{-}bonded/bridge\text{-}type} = I_{multi\text{-}bonded} / I_{bridge\text{-}type}$ (I represented the relative intensity of characteristic peak).

bridge-type adsorbed CO occupied a major part over CCA|ZnO catalyst. Meanwhile, we also found that the CCA|ZnO/ZrO_2 (4:1) possessed a balanced multi-bonded and bridge-type adsorbed CO. The bridge-type adsorbed CO on Co active sites led to the cleavage of C-O bond, promoting the generation of CH_x* intermediates [34]. Therefore, the CCA|ZnO/ZrO_2 (4:1) can provide the suitable amount of CH_x* intermediates due to the proper ZnO/ZrO_2 ratio, compared with CCA|ZnO and CCA|ZrO_2. Recently, Paredes-Nunez et al. [53] had found that in the quantitative operando study of syngas conversion over Co-based catalysts, the formation rate of hydrocarbon (CH_4 and C_3H_6) was lower than or close to the decomposition rate of multi-bonded adsorbed CO. Obviously, the CCA|ZrO_2 catalyst possessed stronger multi-bonded adsorbed CO and showed the lowest total hydrocarbons and CH_4 selectivity (Fig. 11b), while the CCA|ZnO catalyst with the stronger bridge-type adsorbed CO exhibited the higher selectivity of total hydrocarbons and CH_4. Interestingly, the CCA|ZnO/ZrO_2 (4:1) catalyst displayed the medium $I_{multi\text{-}bonded/bridge\text{-}type}$ and the selectivity of total hydrocarbons and CH_4. These results demonstrated that $I_{multi\text{-}bonded/bridge\text{-}type}$ was one of the key factors to affect the hydrocarbons formation. As shown in Fig. S16, *HCOO (1352/1354 cm^{-1}), *CO_3 (1593/1595/1552/1550/1543 cm^{-1}) and *CH_3O (1074/1070 cm^{-1}) over CCA|ZnO/ZrO_2 (4:1), CCA|ZnO and CCA|ZrO_2 catalysts were observed, and they become strong as the reaction temperature increases [22,52]. The *CH_3O species could be obtained by the hydrogenation of *HCOO species [18]. Subsequently, the *CH_3O species were easily dissociated to the CH_x* species [55], which were the key intermediate species for the higher alcohol synthesis.

Generally, the representative enol and CO insertion mechanism with the chain propagation of different intermediate (CH_xO* and CO*) have been used to explain the HAS [3,25,40,56]. Typically, the bridge-type adsorbed CO on Co active sites resulted in the cleavage of C-O bond, which promoted the formation of CH_x* intermediates. In addition, the CH_x* species were generated from the *HCOO and *CH_3O species. And then the C_nH_x* species were formed by the CH_x*- CH_x* coupling

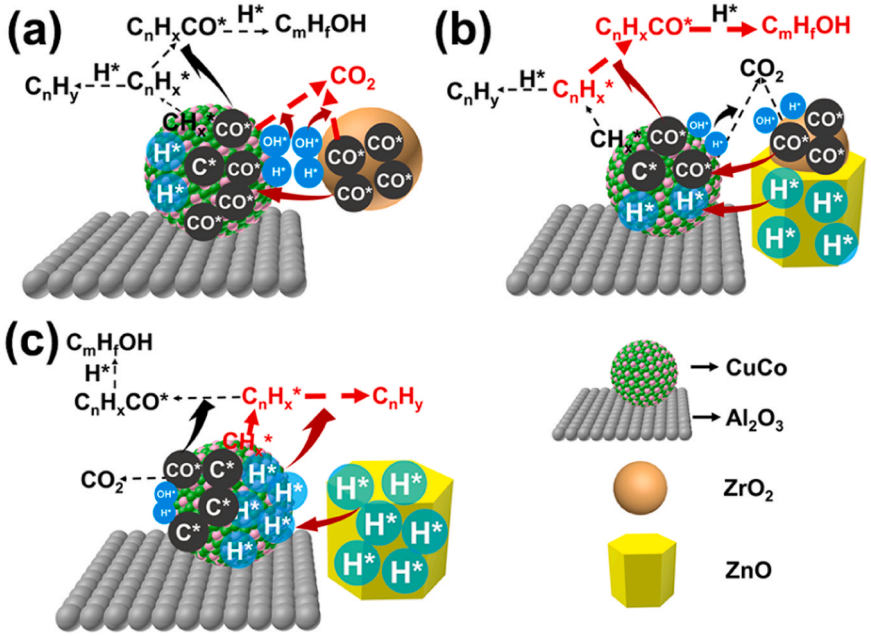

Fig. 12. Schematic illustration of the reaction process of HAS from syngas for the (a) CCA|ZrO_2, (b) CCA|ZnO/ZrO_2 and (c) CCA|ZnO catalyst.

reaction. The Cu active site can non-dissociate CO to form CO*, which subsequently inserts into the C_nH_x* species to obtain higher alcohols. The hydrocarbons were synthesized through the hydrogenation reaction of CH_x* or C_nH_x* species. Combined with the above in situ DRIFTS and chemisorption (CO and H_2) analysis, a cooperative reaction route over the catalysts was proposed (see Fig. 12). For the CCA|ZrO_2 catalyst (Fig. 12a), the formation of CO* species was more than H* species due to that ZrO_2 can be capable of chemisorbing CO. As reported by our previous work [22], ZrO_2 with more oxygen vacancy sites could promote the dissociation of H_2O to to obtain more surface hydroxyl (OH*), which then reacted with the CO* species to form CO_2. The abundant CO* species reacted with more OH* to produce CO_2 rather than reacting with C_nH_x* species to produce alcohols due to the lack of sufficient C_nH_x* species. Simultaneously, the lowest amount of H_2 adsorption also suppressed the hydrocarbon formation. By contrast, over the CCA|ZnO catalyst, ZnO provided larger amount of dissociated hydrogen species through the strong heterolytic dissociation, favoring for the hydrogenation of CH_x* and C_nH_x* species to form hydrocarbons (Fig. 12c). Moreover, only small amount of CO_2 was produced from the water gas shift reaction owing to the deficient CO* species on the catalyst. In terms of the CCA|ZnO/ZrO_2 catalyst (Fig. 12b), the proper amount of ZnO and ZrO_2 got a good compromise between the non-dissociation of CO species and the activation of H_2, maintaining the balance of relative amount of CO*, C_nH_x* and H* species over the catalyst surface. This propelled C_nH_x*-CO* coupling reaction and then led to the enhanced selectivity of higher alcohols accompanied by appropriate formation of hydrocarbons and CO_2.

5. Conclusion

In summary, we have prepared series of CCA|ZnO/ZrO_2 modified catalysts by the mortar-mixing of CuCoAl and ZnO/ZrO_2 composites for the selective synthesis of higher alcohols. Compared with the CCA|ZrO_2 and CCA|ZnO catalysts, the CCA|ZnO/ZrO_2 catalysts presented a volcanic trend of ROH selectivity with the increase of ZnO/ZrO_2 ratio. At ZnO/ZrO_2 ratio of 4:1, the catalyst exhibited the highest ROH selectivity of 42.6 wt% with excellent C_{2+}OH/ROH fraction of 83.7%. Combined various characterization techniques, we found that the surface [H*]/[C*] ratio of CCA|ZnO/ZrO_2 catalysts was inherently related with the STY_{ROH} and ROH selectivity. Excessive or much lower [H*]/[C*] ratio was detrimental to the higher alcohol synthesis owing to the lack of CO* species or CH* species. The CCA|ZnO/ZrO_2 (ZnO/ZrO_2 = 4:1) catalyst with moderate [H*]/[C*] ratio kept a good balance of relative amount of CO*, CH_x* and H* species, promoting the probability of C_nH_x*-CO* coupling reaction and then enhancing the STY_{ROH} and ROH selectivity. Based on the analysis of the structure-performance relationship, the synergistic effect of CuCoAl and ZnO/ZrO_2 on the selective impetus of the reaction network was proposed to clarify the nature of higher alcohol synthesis via syngas over CCA|ZnO/ZrO_2 modified catalysts.

CRediT authorship contribution statement

Chao Huang: Investigation, Data curation, Formal analysis, Methodology, Software, Writing - original draft, Validation, Visualization, Conceptualization. Can Zhu: Formal analysis, Resources, Writing - review & editing, Methodology, Validation. Mingwei Zhang: Writing - review & editing, Validation, Supervision. Jiangang Chen: Resources, Supervision. Kegong Fang: Conceptualization, Funding acquisition, Project administration, Validation, Supervision, Writing - original draft, Writing - review & editing.

Declaration of Competing Interest

The authors declare that they have no known competing financial interests or personal relationships that could have appeared to influence the work reported in this paper.

Acknowledgements

This research was funded by the National Key R&D Program of China (2019YFB1503905).

Appendix A. Supporting information

Supplementary data associated with this article can be found in the online version at doi:10.1016/j.apcatb.2021.120739.

References

[1] K.G. Fang, D.B. Li, M.G. Lin, M.L. Xiang, W. Wei, Y.H. Sun, A short review of heterogeneous catalytic process for mixed alcohols synthesis via syngas, Catal. Today 147 (2009) 133–138.
[2] V.R. Surisetty, A.K. Dalai, J. Kozinski, Alcohols as alternative fuels: an overview, Appl. Catal. A-Gen. 404 (2011) 1–11.
[3] M. Ao, G.H. Pham, J. Sunarso, M.O. Tade, S.M. Liu, Active centers of catalysts for higher alcohol synthesis from syngas: a review, ACS Catal. 8 (2018) 7025–7050.
[4] C. Huang, M.W. Zhang, C. Zhu, X.L. Mu, K. Zhang, L.S. Zhong, K.G. Fang, M.H. Wu, Fabrication of highly stable SiO_2 encapsulated multiple CuFe nanoparticles for higher alcohols synthesis via CO hydrogenation, Catal. Lett. 148 (2018) 1080–1092.
[5] Y.Z. Xiang, R. Barbosa, N. Kruse, Higher alcohols through CO hydrogenation over CoCu catalysts: influence of precursor activation, ACS Catal. 4 (2014) 2792–2800.
[6] G. Prieto, S. Beijer, M.L. Smith, M. He, Y. Au, Z. Wang, D.A. Bruce, K.P. de Jong, J. J. Spivey, P.E. de Jongh, Design and synthesis of copper-cobalt catalysts for the selective conversion of synthesis gas to ethanol and higher alcohols, Angew. Chem. -Int. Ed. 53 (2014) 6397–6401.
[7] X.Y. Han, K.G. Fang, J. Zhou, L. Zhao, Y.H. Sun, Synthesis of higher alcohols over highly dispersed Cu-Fe based catalysts derived from layered double hydroxides, J. Colloid Interface Sci. 470 (2016) 162–171.
[8] F.S. Toniolo, R. Magalhaes, C.A.C. Perez, M. Schmal, Structural investigation of $LaCoO_3$ and $LaCoCuO_3$ perovskite-type oxides and the effect of Cu on coke deposition in the partial oxidation of methane, Appl. Catal. B-Environ. 117 (2012) 156–166.
[9] E. Heracleous, E.T. Liakakou, A.A. Lappas, A.A. Lemonidou, Investigation of K-promoted Cu-Zn-Al, Cu-X-Al and Cu-Zn-X (X = Cr, Mn) catalysts for carbon monoxide hydrogenation to higher alcohols, Appl. Catal. A-Gen. 455 (2013) 145–154.
[10] Y.J. Liu, N. Cui, P.L. Jia, X. Wang, W. Huang, Synergy between active sites of ternary CuZnAlOOH Catalysts in CO hydrogenation to ethanol and higher alcohols, ACS Sustain. Chem. Eng. 8 (2020) 6634–6646.
[11] J. Yong, X. Luan, X. Dai, X. Zhang, Y. Yang, H. Zhao, M. Cui, Z. Ren, F. Nie, X. Huang, Alkaline-etched NiMgAl trimetallic oxide-supported KMoS-based catalysts for boosting higher alcohol selectivity in CO hydrogenation, ACS Appl. Mater. Interfaces 11 (2019) 19066–19076.
[12] V.R. Surisetty, A. Tavasoli, A.K. Dalai, Synthesis of higher alcohols from syngas over alkali promoted MoS_2 catalysts supported on multi-walled carbon nanotubes, Appl. Catal. A-Gen. 365 (2009) 243–251.
[13] N.Y. Yang, A.J. Medford, X.Y. Liu, F. Studt, T. Bligaard, S.F. Bent, J.K. Norskov, Intrinsic selectivity and structure sensitivity of rhodium catalysts for C_{2+} oxygenate production, J. Am. Chem. Soc. 138 (2016) 3705–3714.
[14] N.D. Subramanian, J. Gao, X. Mo, J.G. Goodwin Jr., W. Torres, J.J. Spivey, La and/or V oxide promoted Rh/SiO_2 catalysts: effect of temperature, H_2/CO ratio, space velocity, and pressure on ethanol selectivity from syngas, J. Catal. 272 (2010) 204–209.
[15] A. Bordoloi, J. Anton, H. Ruland, M. Muhler, S. Kaluza, Metal-support interactions in surface-modified Cu-Co catalysts applied in higher alcohol synthesis, Catal. Sci. Technol. 5 (2015) 3603–3612.
[16] W. Gao, Y.F. Zhao, H.R. Chen, H. Chen, Y.W. Li, S. He, Y.K. Zhang, M. Wei, D. G. Evans, X. Duan, Core-shell Cu@(CuCo-alloy)/Al_2O_3 catalysts for the synthesis of higher alcohols from syngas, Green. Chem. 17 (2015) 1525–1534.
[17] G.L. Liu, Y.X. Geng, D.M. Pan, Y. Zhang, T. Niu, Y. Liu, Bi-metal Cu-Co from $LaCo_{1-x}Cu_xO_3$ perovskite supported on zirconia for the synthesis of higher alcohols, Fuel Process. Technol. 128 (2014) 289–296.
[18] K. Sun, Y.Q. Wu, M.H. Tan, L.Y. Wang, G.H. Yang, M. Zhang, W. Zhang, Y.S. Tan, Ethanol and higher alcohols synthesis from syngas over CuCoM (M=Fe, Cr, Ga and Al) nanoplates derived from hydrotalcite-Like precursors, ChemCatChem 11 (2019) 2695–2706.
[19] L. Zhao, W.B. Li, J. Zhou, X.L. Mu, K.G. Fang, One-step synthesis of Cu-Co alloy/Mn_2O_3-Al_2O_3 composites and their application in higher alcohol synthesis from syngas, Int. J. Hydrogen Energy 42 (2017) 17414–17424.
[20] X. Liu, W. Zhou, Y. Yang, K. Cheng, J. Kang, L. Zhang, G. Zhang, X. Min, Q. Zhang, Y. Wang, Design of efficient bifunctional catalysts for direct conversion of syngas into lower olefins via methanol/dimethyl ether intermediates, Chem. Sci. 9 (2018) 4708–4718.
[21] K. Cheng, B. Gu, X. Liu, J. Kang, Q. Zhang, Y. Wang, Direct and highly selective conversion of synthesis gas into lower olefins: design of a bifunctional catalyst combining methanol synthesis and carbon-carbon coupling, Angew. Chem. -Int. Ed. 55 (2016) 4725–4728.

[22] C. Huang, C. Zhu, M. Zhang, Y. Lu, Q. Wang, H. Qian, J. Chen, K. Fang, Direct conversion of syngas to higher alcohols over a CuCoAl|t-ZrO_2 multifunctional catalyst, ChemCatChem 13 (2021) 3184–3197.
[23] A.B. Anderson, J.A. Nichols, Hydrogen on zinc-oxide - theory of its heterolytic adsorption, J. Am. Chem. Soc. 108 (1986) 4742–4746.
[24] T.J. Lin, X.Z. Qi, X.X. Wang, L. Xia, C.Q. Wang, F. Yu, H. Wang, S.G. Li, L.S. Zhong, Y.H. Sun, Direct production of higher oxygenates by syngas conversion over a multifunctional catalyst, Angew. Chem. Int. Ed. 58 (2019) 4627–4631.
[25] X. Luan, Z. Ren, X. Dai, X. Zhang, J. Yong, Y. Yang, H. Zhao, M. Cui, F. Nie, X. Huang, Selective conversion of syngas into higher alcohols via a reaction-coupling strategy on multifunctional relay catalysts, ACS Catal. 10 (2020) 2419–2430.
[26] J. Ni, W.H. Leng, J. Mao, J.G. Wang, J.Y. Lin, D.H. Jiang, X.N. Li, Tuning electron density of metal nickel by support defects in Ni/ZrO_2 for selective hydrogenation of fatty acids to alkanes and alcohols, Appl. Catal. B-Environ. 253 (2019) 170–178.
[27] X. Gao, T. Zhang, Y. Wu, G. Yang, M. Tan, X. Li, H. Xie, J. Pan, Y. Tan, Isobutanol synthesis from syngas on Zn-Cr based catalysts: new insights into the effect of morphology and facet of ZnO nanocrystal, Fuel 217 (2018) 21–30.
[28] J. Wang, G. Li, Z. Li, C. Tang, Z. Feng, H. An, H. Liu, T. Liu, C. Li, A highly selective and stable ZnO-ZrO_2 solid solution catalyst for CO_2 hydrogenation to methanol, Sci. Adv. 3 (2017), 1701290.
[29] T. Wang, C. Yang, P. Gao, S. Zhou, S. Li, H. Wang, Y. Sun, $ZnZrO_x$ integrated with chain-like nanocrystal HZSM-5 as efficient catalysts for aromatics synthesis from CO_2 hydrogenation, Appl. Catal. B: Environ. 286 (2021), 119929.
[30] Z. Lu, H. Yin, A. Wang, J. Hu, W. Xue, H. Yin, S. Liu, Hydrogenation of ethyl acetate to ethanol over Cu/ZnO/MO_x (MO_x=SiO_2, Al_2O_3, and ZrO_2) catalysts, J. Ind. Eng. Chem. 37 (2016) 208–215.
[31] X. Mo, Y.-T. Tsai, J. Gao, D. Mao, J.G. Goodwin, Effect of component interaction on the activity of Co/CuZnO for CO hydrogenation, J. Catal. 285 (2012) 208–215.
[32] M. Bahmani, B. Vasheghani Farahani, S. Sahebdelfar, Preparation of high performance nano-sized Cu/ZnO/Al_2O_3 methanol synthesis catalyst via aluminum hydrous oxide sol, Appl. Catal. A: Gen. 520 (2016) 178–187.
[33] A.G. Sato, D.P. Volanti, D.M. Meira, S. Damyanova, E. Longo, J.M.C. Bueno, Effect of the ZrO_2 phase on the structure and behavior of supported Cu catalysts for ethanol conversion, J. Catal. 307 (2013) 1–17.
[34] K. Sun, X.F. Gao, Y.X. Bai, M.H. Tan, G.H. Yanga, Y.S. Tan, Synergetic catalysis of bimetallic copper-cobalt nanosheets for direct synthesis of ethanol and higher alcohols from syngas, Catal. Sci. Technol. 8 (2018) 3936–3947.
[35] S.J. Han, G. Park, Y.-J. Lee, K.-W. Jun, S.K. Kim, Y.T. Kim, G. Kwak, Higher alcohol synthesis from syngas over xerogel-derived Co-Cu-Al_2O_3 catalyst with an enhanced metal proximity, Mol. Catal. 475 (2019), 110481.
[36] K. Sun, M.H. Tan, Y.X. Bai, X.F. Gao, P. Wang, N.N. Gong, T. Zhang, G.H. Yang, Y. S. Tan, Design and synthesis of spherical-platelike ternary copper-cobalt-manganese catalysts for direct conversion of syngas to ethanol and higher alcohols, J. Catal. 378 (2019) 1–16.
[37] F. Morales, F.M.F. de Groot, O.L.J. Gijzeman, A. Mens, O. Stephan, B. M. Weckhuysen, Mn promotion effects in Co/TiO_2 Fischer-Tropsch catalysts as investigated by XPS and STEM-EELS, J. Catal. 230 (2005) 301–308.
[38] X.Y. Jia, X.S. Zhang, N. Rui, X. Hu, C.J. Liu, Structural effect of Ni/ZrO_2 catalyst on CO_2 methanation with enhanced activity, Appl. Catal. B-Environ. 244 (2019) 159–169.
[39] Y. Wang, W. Zhan, Z. Chen, J. Chen, X. Li, Y. Li, Advanced 3D hollow-out ZnZrO@C combined with hierarchical zeolite for highly active and selective CO hydrogenation to aromatics, ACS Catal. 10 (2020) 7177–7187.
[40] D. Xu, M. Ding, X. Hong, G. Liu, Mechanistic aspects of the role of K promotion on Cu-Fe-based catalysts for higher alcohol synthesis from CO_2 hydrogenation, ACS Catal. 10 (2020) 14516–14526.
[41] J.J. Su, Z.P. Zhang, D.L. Fu, D. Liu, X.C. Xu, B.F. Shi, X. Wang, R. Si, Z. Jiang, J. Xu, Y.F. Han, Higher alcohols synthesis from syngas over CoCu/SiO_2 catalysts: dynamic structure and the role of Cu, J. Catal. 336 (2016) 94–106.
[42] C. Qin, B. Hou, J.G. Wang, Q. Wang, G. Wang, M.T. Yu, C.B. Chen, L.T. Jia, D.B. Li, Crystal-plane-dependent Fischer-Tropsch performance of cobalt catalysts, ACS Catal. 8 (2018) 9447–9455.
[43] T. Ishida, T. Yanagihara, X. Liu, H. Ohashi, A. Hamasaki, T. Honma, H. Oji, T. Yokoyama, M. Tokunaga, Synthesis of higher alcohols by Fischer-Tropsch synthesis over alkali metal-modified cobalt catalysts, Appl. Catal. A-Gen. 458 (2013) 145–154.
[44] G. Aguila, S. Guerrero, P. Araya, Influence of the crystalline structure of ZrO_2 on the activity of Cu/ZrO_2 catalysts on the water gas shift reaction, Catal. Commun. 9 (2008) 2550–2554.
[45] C.Q. Chen, C.X. Ruan, Y.Y. Zhan, X.Y. Lin, Q. Zheng, K.M. Wei, The significant role of oxygen vacancy in Cu/ZrO_2 catalyst for enhancing water-gas-shift performance, Int. J. Hydrogen Energy 39 (2014) 317–324.
[46] Y.F. Zhang, L.S. Zhong, H. Wang, P. Gao, X.P. Li, S. Xiao, G.J. Ding, W. Wei, Y. H. Sun, Catalytic performance of spray-dried Cu/ZnO/Al_2O_3/ZrO_2 catalysts for slurry methanol synthesis from CO_2 hydrogenation, J. CO2 Util. 15 (2016) 72–82.
[47] O.D. Pavel, D. Tichit, I.-C. Marcu, Acido-basic and catalytic properties of transition-metal containing Mg-Al hydrotalcites and their corresponding mixed oxides, Appl. Clay Sci. 61 (2012) 52–58.
[48] J.Z. Lu, L.J. Yang, B.L. Xu, Q. Wu, D. Zhang, S.J. Yuan, Y. Zhai, X.Z. Wang, Y. N. Fan, Z. Hu, Promotion effects of nitrogen doping into carbon nanotubes on supported Iron Fischer-Tropsch catalysts for lower olefins, ACS Catal. 4 (2014) 613–621.
[49] C. Zhu, M. Zhang, C. Huang, Y. Han, K. Fang, Controlled nanostructure of zeolite crystal encapsulating FeMnK catalysts targeting light olefins from syngas, ACS Appl. Mater. Interfaces 12 (2020) 57950–57962.
[50] H. Suo, S. Wang, C. Zhang, J. Xu, B. Wu, Y. Yang, H. Xiang, Y.W. Li, Chemical and structural effects of silica in iron-based Fischer–Tropsch synthesis catalysts, J. Catal. 286 (2012) 111–123.
[51] X. Li, Y. Chen, M.U. Nisa, Z. Li, Combating poison with poison-Irreducible Co_2SiO_4 as a promoter to modify Co-based catalysts in Fischer-Tropsch synthesis, Appl. Catal. B: Environ. 267 (2020), 118377.
[52] D. Xu, H. Yang, X. Hong, G. Liu, S.C. Edman Tsang, Tandem catalysis of direct CO_2 hydrogenation to higher alcohols, ACS Catal. 11 (2021) 8978–8984.
[53] A. Paredes-Nunez, D. Lorito, L. Burel, D. Motta-Meira, G. Agostini, N. Guilhaume, Y. Schuurman, F. Meunier, CO hydrogenation on cobalt-based catalysts: tin poisoning unravels CO in hollow sites as a main surface intermediate, Angew. Chem. -Int. Ed. 57 (2018) 547–550.
[54] C.J. Weststrate, J. van de Loosdrecht, J.W. Niemantsverdriet, Spectroscopic insights into cobalt-catalyzed Fischer-Tropsch synthesis: A review of the carbon monoxide interaction with single crystalline surfaces of cobalt, J. Catal. 342 (2016) 1–16.
[55] C. Yang, R. Mu, G. Wang, J. Song, H. Tian, Z.-J. Zhao, J. Gong, Hydroxyl-mediated ethanol selectivity of CO_2 hydrogenation, Chem. Sci. 10 (2019) 3161–3167.
[56] J. Su, W. Mao, X.-C. Xu, Z. Yang, H. Li, J. Xu, Y.-F. Han, Kinetic study of higher alcohol synthesis directly from syngas over CoCu/SiO_2 catalysts, Aiche J. 60 (2014) 1797–1809.